Improved Hydrate Equilibrium Measurements in Ternary Gas and Black Oil Systems

J. Ivanic, Z. Huo, and E.D. Sloan
Center for Hydrate Research, Colorado School of Mines, Golden, CO 80401
Email Correspondent: ESloan@mines.edu

Abstract

This work shows that hydrate formation in black oil systems can be incorrectly predicted for two major reasons: (1) a large degree of metastability associated with hydrate formation and dissociation and (2) a previously unconsidered effect of water cut on the water activity and hydrocarbon bubble-point. A new experimental technique is introduced to accurately assess the pressure-temperature equilibrium. A third and forth reason for prediction discrepancies, those of accurate oil characterization and hydrate structural change, await future assessment.

1. Introduction

Current hydrate predictions programs consistently show inaccuracy in predicting complex systems such as black oils. For certain black oils, Hopgood (2001) states that experimental data are under-predicted by more than 10^{o}F. This presents a large economic concern when these programs are used in pipeline design and in determining the amounts of inhibitor required for optimal pipeline operation. Four possible sources of error in the current prediction models are: (1) phase metastability leading to inaccurate measurements, (2) an inaccurate prediction of the hydrocarbon fugacities due to

incompletely characterized petroleum fractions, (3) inaccurate aqueous phase activities, or (4) faulty hydrate structure predictions.

Traditional hydrate equilibrium measurements consist of forming hydrates and then measuring the hydrate-vapor-liquid water equilibrium conditions under which the last hydrate crystal is dissociated by heating the system.

Preliminary experiments in this work agree with Tohidi (2000), that the traditional method of measuring hydrate equilibrium can be erroneous when the dissociation metastability is not considered. If the system is heated too rapidly (this can be as slow as 0.15K/hr), the system can exhibit metastability of dissociation and true equilibrium will not be established, thereby producing hydrate equilibrium data that can be more than 3K higher in temperature than the actual equilibrium at a given pressure.

2. Experimental Apparatus.

The experimental apparatus shown in Figure 1 is one of two identical cells in which all equilibrium experiments were performed. Each $0.2m^3$ bath was heated with two, 120-watt Vycor® glass emersion heaters and cooled with a Blue M constant-flow portable cooling unit. The temperature range of the experiments was 274K to 300K. The two identical high-pressure cells are MagnaDrive®, bolted-closure autoclaves, constructed of stainless steel with volumes of 300 cm^3 and working pressures of 35MPa. Each uses a 0.75 horsepower Dayton DC motor with a maximum agitation speed of 2500 rpm, but a nominal 400 rpm was typically used.

Temperature measurements in the cell and in the bath were taken with Omega thermistor probes with a 0.1^oF error. Pressure measurements in the cells were taken with

Sensotec pressure transducers with an error of 5%. The pressure and temperature were continuously controlled and measured using a Mistic® Controller and Cyrano® 200 software.

Autoclave Engineering fittings were used with 1/8 inch stainless steel piping. A one horsepower Leybold-Heraeus vacuum pump was used to evacuate the cells and a Ruska hand-pump was used to inject water into a piston cylinder, which would displace oil into the cell. For natural gas systems, the piston cylinder was replaced with a pressurized cylinder.

2 Experimental Method

The traditional method of measuring hydrate equilibrium consists of monitoring the pressure and temperature in a hydrate-bearing system and identifying equilibrium at the conditions where the last hydrate crystal in the system dissociates. This procedure is illustrated in Figure 2, which shows the typical pressure-temperature trace produced during a hydrate equilibrium measurement.

Following the trace from segment A to D, the experimental procedure may be explained. Over Segment A of Figure 2 the system was isometrically cooled. This linear segment was produced from a hydrate-free system. The system was subcooled well past the hydrate formation conditions. Segment B shows the characteristic pressure drop associated with the exothermic formation of the hydrate phase. Once the hydrate phase formed, the system was heated at a constant rate along Segment C until the pressure-temperature trace coincided with Segment A, the hydrate-free system, and the last hydrate dissociated. The hydrate equilibrium point was assumed to occur at the

conditions at which Segment C meet Segment D. Lastly, the system was further heated to check that Segment D coincided with Segment A; the final conditions are equal to the initial conditions.

The problem with the above method is that a large region of metastability exists. To reduce the error the same general method is used, but the metastability associated with both formation and dissociation is reduced. Figure 3 is a pressure-temperature trace similar to Figure 2, except that it consists of increasingly smaller loops. This is the heart of the method used to measure hydrate equilibrium conditions in this work. Each loop shows a smaller difference between the onset of hydrate formation and the end of hydrate dissociation.

Beginning a loop immediately after the last hydrate dissociated from the previous loop produced successively smaller loops. This was hypothesized to be due to residual liquid hydrate cage structures immediately available upon hydrate dissociation, to reduce the metastability associated with hydrate formation. After the last hydrate is dissociated, many hydrogen bonds and partial cages are still intact. If one continued to heat the system well beyond the hydrate equilibrium conditions (e.g. 286K), all of the residual bonds/cages would be broken. By immediately cooling the system again, one can retain residual structures. This will reduce the metastability associated with the subsequent formation of a hydrate phase, as less energy and entropy are required for cage nucleation and growth. For each sequential loop hydrate formation will occur at a higher temperature and the dissociation will occur at a lower temperature, thereby reducing the degree of metastability of the experiment.

Once a distinct pressure drop indicates hydrate formation, the system is heated to a temperature lower than the previously measured equilibrium temperature. It is important that minimal hydrates are formed to reduce both the metastability and the experimental time. The temperature is held constant as hydrates dissociate. If complete dissociation does not occur, as indicated by the merging of formation and dissociation lines, the temperature is increased slightly and again held constant. This is repeated until complete dissociation occurs.

Once complete dissociation is recorded, the process is repeated in increasingly smaller pressure-temperature loops to reduce metastability. The smaller the loop - the more accurate the results. The limit is obtained when a smaller loop cannot be produced due to the system's inherent metastability. The final dissociation point with the smallest loop is the measured equilibrium point. Complex systems, such as those involving black oils may require more than 10 loops and the metastability may still be greater than 1K. These experiments can last from 1 to 4 days depending upon the complexity of the system.

3. Experimental Results

In early experiments hydrates were formed from a synthetic Green Canyon Gas (GCG) with a composition given in Table 1. This system was chosen because it simulates an industrial multi-component natural gas, and because the equilibrium conditions in the literature for this gas differed from the predictions by as much as 2.8K.

Results, shown in Figure 4, were obtained using both traditional and new experimental methods. The data collected using the traditional method lay to the right of

the predictions, as expected, with a difference between 2.2K and 2.8K. These data matched existing literature data, (Kotkoskie, 1992), for reasons that are discussed in the next section. The data collected with the new experimental method matched the predictions within the error of the experiment except for the point at the lowest pressure and temperature.

In the GCG experiments, the metastability was reduced to 0.3K. This is a best-case scenario and the equilibrium measurement cannot increase much more in accuracy. Shown in Figure 5 is a characteristic pressure-temperature trace for the GCG + Water system. It shows that the metastability can be reduced to 0.3K.

Hydrate equilibrium measurements for the black oil systems proved to be experimentally difficult and time consuming. Accurate data was collected for 3 different black oils. Tables 2, 3, and 4 were prepared by Westport Technology Center and are characterizations for Black Oil A (BOA), Black Oil B (BOB), and Black Oil C (BOC) respectively. Figure 6 shows the results for the black oils used in this work along with the pressure-temperature conditions for hydrate equilibrium of each oil. The experimental results agree well with the predictions. Unexpectedly, the experimental results lay to the left and to the right of the predictions. The experimental data were expected to lie to the right of the predictions, since the metastability of black oil systems is very difficult to reduce below 0.5K. These results also show a change in the curvature of the hydrate equilibrium envelope above the bubble point of the oil. Further explanations of these observations are in the Section 4, Discussion of Results.

X-ray diffraction measurements for BOA and BOC are shown in Figures 7 and 8, respectively. Both of these oils formed sII hydrates as illustrated via a comparison with a

methane-propane hydrate pattern, which is a known structure II hydrate. The structure of hydrates formed form BOB was not measured, due to sample difficulties.

4.4. Discussion of Results

Figure 4 shows that data from Kotkoskie (1992) for GCG were replicated using the traditional method in the current work. Heating rates ranging from 0.15K per hour to 2.8K per hour were used to obtain data with the traditional method. The different heating rates within this range did not produce different data. Also shown in Figure 4 are data obtained via the new experimental method which agree with the predictions within the experimental error of the measurements, except for the point at the lowest pressure. The new experimental method appears to produce data that are more consistent with the predictions than the traditional method.

Data for 3 black oil systems were collected and compared with predictions, shown in Figure 6. The horizontal error bars represent the error in the experiment from the metastability of the oil and the vertical error bars represent the error in the pressure measurements. Error in the temperature measurements is equivalent to the size of the data points. The true equilibrium lay within the range of the metastability.

Black Oil A (BOA) was the oil that showed the least amount of metastability - only 0.5K. The experimental results for BOA lay to the left of the predictions, which is uncommon. This suggests that the predictions may be inaccurate.

Black Oil C (BOC) showed a different trend when compared to predictions. The experimental data was under-predicted at low pressures and over-predicted at high pressures. The under-predicted data may be inaccurate due to the larger amount of metastability associated with BOC, which was 1K or greater; this would imply that the

data should be under-predicted throughout the entire range of data, yet this is not the case. Since the model does not consistently under-predict the data, there appears to be errors associated with the prediction of BOC.

For Black Oil B (BOB), the last of the three oils tested, predictions agreed with the data collected. Figure 9 shows the experimental results and predictions for BOB in greater detail. The data are predicted very well below and above the bubble point. Above the bubble point, data exist for two water cuts (52% and 77%). The predictions very accurately predict the effect of water cut for this oil.

When dealing with such complex systems as black oils, the error may derive from a number of sources. One of the simplest sources of error is the identification of the oil's components. Oil is generally only fully specified in composition below iso-pentane and normal pentane. Beyond that the remaining pentanes, hexanes, heptanes and heavier components are lumped into fractions, and each fraction is represented by a pseudo-component. Work by Rasmussen & Pedersen (2002) has shown that the heavy structure II hydrate formers are non-negligible when predicting hydrate equilibrium.

There are also physical limitations of the experiment. There is an inherent degree of metastability that is difficult to eliminate within a practical timescale of an experiment. Also, with the large cell used in this work, mass transfer through the oil phase is slow, impeding equilibrium from being quickly established. In the cell, the gas phase needs to communicate with the aqueous phase through the oil phase. A smaller cell volume with increased agitation would reduce this experimental difficulty.

Another significant source of error is the inaccurate prediction of the oil bubble-point. The experimental data and the predictions in Figure 9 show a change in the slope

and curvature of the hydrate equilibrium envelope for BOB. The envelope changes from a four-phase exponential curve (vapor-aqueous liquid-liquid hydrocarbon-hydrate) to a steeper-sloped, three-phase line (aqueous liquid–liquid hydrocarbon-hydrate) just above 4MPa. This is the point at which the vapor phase condenses completely to a liquid hydrocarbon phase. In Figure 9 the effect of bubble-point is shown to be a function of water cut.

Figure 10 shows that for water cuts greater than 60%, a substantial shift to the left in the hydrate phase envelope is predicted. This is the result of the bubble-point being depressed, causing the four-phase envelope (vapor-aqueous liquid-liquid hydrocarbon-hydrate) to change to a three-phase envelope (aqueous liquid–liquid hydrocarbon-hydrate) earlier. The bubble-point is a function of the system composition, which may be predicted erroneously at high water cuts. It is hypothesized that the bubble-point is depressed with increasing water cut, due to the aqueous phase dissolution of lighter components from the gas phase. As the lighter gas phase components are consumed, the remaining heavier vapor-liquid hydrocarbons depress the vapor pressure or bubble-point. The activities of the aqueous phase need to be well known in order to correctly predict this behavior.

An incorrect oil composition could account for prediction errors above and below the bubble-point. Incorrect bubble-point predictions, however, would only produce errors above the bubble-point.

In general, a more methodical approach to black oil systems is necessary if any type of correlation is to be drawn between its components/fractions and the hydrate systems it forms. Due to the anecdotal submittal of black oils tested thus far, this has not

been the case. Rather than simply analyzing anecdotal oils, oils with systematic variations in compositions must be studied to obtain data suitable for correlations describing the "majority" of black oil systems.

5. Conclusions

When measuring the hydrate equilibrium conditions for increasingly complex systems, it is vital to eliminate the metastability associated with the experiment. A modified experimental technique was developed to eliminate the metastability associated with hydrate formation and dissociation. Using this experimental technique it is shown that the amount of metastability can be reduced to as little as 0.28K (for a multi-component natural gas system), approaching the error of the experiment. Current models (CSMGem® and PVTsim®) in fact predict hydrate equilibrium accurately for such earlier mentioned systems of multi-component natural gases and black oils within 0.5K.

Further work on controlled black oil systems must be performed to gain a better fundamental understanding of their behavior as whole, in addition to the contribution of each of their many components. Many studies thus far have been performed on "outlier" systems; that is, black oils which tend to give interesting, but unexpected results. However, to form the basis of any engineering correlation, a methodical study of black oils must be performed in which the deviation amongst oils is small, and the oils behave according to, rather than the exception to, the "rules" governing typical hydrate formation.

The effect of water cut should be investigated. The experiments in this work show that hydrate equilibrium, for the systems considered in this work, is a function of

water cut. Although predictions show the same trend as the experiments, if the bubble point is incorrectly predicted due the effects of high water cuts, inaccuracies will exist. If the activities of the aqueous phase are not well known, predictions for the compositions of the vapor and liquid water phases will be inaccurate. This leads to inaccurate bubble-point predictions. Further experiments are necessary to determine how accurately these shifts are predicted.

6. Acknowledgements

We are grateful to Phil Notz, Siva Subramanian, and DeepStar for their advice and support on this project.

References

Hopgood, D. "Why Improve Hydrate Predictions for Deepwater Black Oil?" Proc. Offshore Technology Conference, OTC 13037, 30 April – 3 May (2001).

Kotkoskie, T.S., B. Al-Ubaidi, et al. (1992). "Inhibition of Gas Hydrates in Water-Based Drilling Muds." SPE Drilling Engineering: 130-136.

Rasmussen, C. P., & Pedersen, K. S., (2002). Challenges in Modeling Gas Hydrate Phase Equilibria. *Proceedings of the 4th International Conference on Gas Hydrates* **1**, 388-393.

Tohidi, B., R. Burgass, et al. (2000). "Improving the accuracy of gas hydrate dissociation point measurements." Gas hydrates, challenges for the future NYAS 912:924.

Tables and Figures

Table 1 Green Canyon Gas Composition

Green Canyon Gas (GCG) Composition	
Component	Mole Fraction
C1	87.2
C2	7.6
C3	3.1
i-C4	0.5
n-C4	0.8
i-C5	0.2
n-C5	0.2
N_2	0.4

Table 2 BOA Characterization

Fluid	Wt%	Mole%	Mw (Literature)
N2	0.063	0.223	28.014
CO2	0.005	0.011	44.01
C1	8.866	54.77	16.043
C2	1.381	4.552	30.07
C3	0.666	1.497	44.097
i-C4	0.152	0.259	58.124
n-C4	0.261	0.445	58.124
i-C5	0.193	0.265	72.151
n-C5	0.214	0.294	72.151
C6	0.745	0.857	86.178
Benzene	0.009	0.011	78.114
Toluene	0.065	0.07	92.141
C7	1.992	2.056	96
C8	3.533	3.272	107
C9	3.735	3.059	121
C10	3.95	2.921	134
C11	3.849	2.595	147
C12	2.986	1.838	161
C13	3.926	2.223	175
C14	3.286	1.714	190
C15	3.336	1.605	206
C16	3.271	1.46	222
C17	2.964	1.239	237
C18	3.131	1.236	251
C19	2.535	0.955	263
C20	2.612	0.941	275
C21	2.332	0.794	291
C22	2.283	0.742	305
C23	2.461	0.767	318
C24	1.668	0.499	331
C25	1.777	0.51	345
C26	2.139	0.59	359
C27	1.756	0.465	374
C28	1.734	0.443	388
C29	1.653	0.408	402
C30+	24.471	4.414	550
Total	**100**	**100**	
Properties	**Exp**	**Cal**	
GOR (scf/stb)	810	784	
Bubble Point	(300 ^{o}F, 4840 Psi) (202 ^{o}F, 4740 Psi) (120 ^{o}F, 4616 Psi) (80 ^{o}F, 4497 Psi) (40 ^{o}F, 4416 Psi)	(300 ^{o}F, 5186 Psi) (202 ^{o}F, 5108 Psi) (120 ^{o}F, 4827 Psi) (80 ^{o}F, 4605 Psi) (40 ^{o}F, 4317 Psi)	
Density (g/cc)	0.7749	0.7627	at (71.6 ^{o}F, 5500 Psi)

Table 3 BOB Characterization

Fluid	Wt%	Mole%	Mw (Literature)
N2	0.033	0.262	28.013
CO2	0.279	1.429	44.01
C1	1.617	22.694	16.043
C2	0.234	1.755	30.07
C3	0.181	0.923	44.097
i-C4	0.113	0.436	58.123
n-C4	0.253	0.981	58.123
i-C5	0.205	0.639	72.15
n-C5	0.257	0.803	72.15
C6	0.536	1.436	84
Benzene	0.005	0.013	78.12
Toluene	0.012	0.029	92.15
C7	0.806	1.891	96
C8	1.282	2.696	107
C9	1.402	2.608	121
C10	1.625	2.730	134
C11	1.781	2.727	147
C12	2.024	2.830	161
C13	2.584	3.324	175
C14	2.724	3.227	190
C15	2.921	3.192	206
C16	2.759	2.798	222
C17	2.577	2.447	237
C18	2.707	2.428	251
C19	2.587	2.214	263
C20	2.450	2.005	275
C21	2.183	1.688	291
C22	2.171	1.602	305
C23	2.006	1.420	318
C24	1.946	1.323	331
C25	1.896	1.237	345
C26	1.725	1.082	359
C27	1.886	1.135	374
C28	1.926	1.117	388
C29	1.927	1.079	402
C30+	48.379	19.799	550
Total		**100**	
Properties	**Exp**	**Cal**	
GOR (scf/stb)	146	144	
Bubble Point	(120 ^{o}F, 1254 Psi) (80 ^{o}F, 1143 Psi) (40 ^{o}F, 1017 Psi)	(120 ^{o}F, 1135 Psi) (80 ^{o}F, 997 Psi) (40 ^{o}F, 842 Psi)	
Density (g/cc)	0.8955	0.8281	at (150 ^{o}F, 5000 Psi)

Table 4 BOC Characterization

Fluid	Wt%	Mole%	Mw(Literature)
N2	0.0340	0.2060	28.0
CO2	0.0020	0.0060	44.0
C1	3.2980	35.2340	16.0
C2	0.4900	2.7920	30.1
C3	0.2710	1.0520	44.1
IC4	0.0550	0.1630	58.1
NC4	0.0890	0.2620	58.1
IC5	0.0530	0.1250	72.2
NC5	0.0950	0.2260	72.2
C6	0.6560	1.3050	84.0
Benzene	0.0210	0.0450	78.1
Toluene	0.0780	0.1450	92.2
C7	1.7330	3.0950	96.0
C8	2.7690	4.4360	107.0
C9	3.1560	4.4710	121.0
C10	3.2840	4.2000	134.0
C11	2.9350	3.4220	147.0
C12	2.6240	2.7940	161.0
C13	2.7040	2.6480	175.0
C14	2.6150	2.3590	190.0
C15	2.5640	2.1330	206.0
C16	2.3110	1.7840	222.0
C17	2.2680	1.6400	237.0
C18	2.2040	1.5050	251.0
C19	2.1080	1.3740	263.0
C20	1.9830	1.2360	275.0
C21	1.8590	1.0950	291.0
C22	1.8030	1.0130	305.0
C23	1.6900	0.9110	318.0
C24	1.5760	0.8160	331.0
C25	1.5380	0.7640	345.0
C26	1.4660	0.7000	359.0
C27	1.4730	0.6750	374.0
C28	1.4510	0.6410	388.0
C29	1.3860	0.5910	402.0
C30+	45.3610	14.1360	550.0
Total	**100.0**	**100.0**	
Properties	**Exp**	**Cal**	
GOR (scf/stb)	267	268	
Bubble Point	(120 ^{o}F, 1945 Psi) (80 ^{o}F, 1810 Psi) (71 ^{o}F, 1755 Psi) (40 ^{o}F, 1650 Psi)	(120 F, 1919 Psi) (80 F, 1705 Psi) (71 F, 1650 Psi) (40 F, 1454 Psi)	
Density (g/cc)	0.8432	0.7952	at (155 ^{o}F, 5000 Psi)

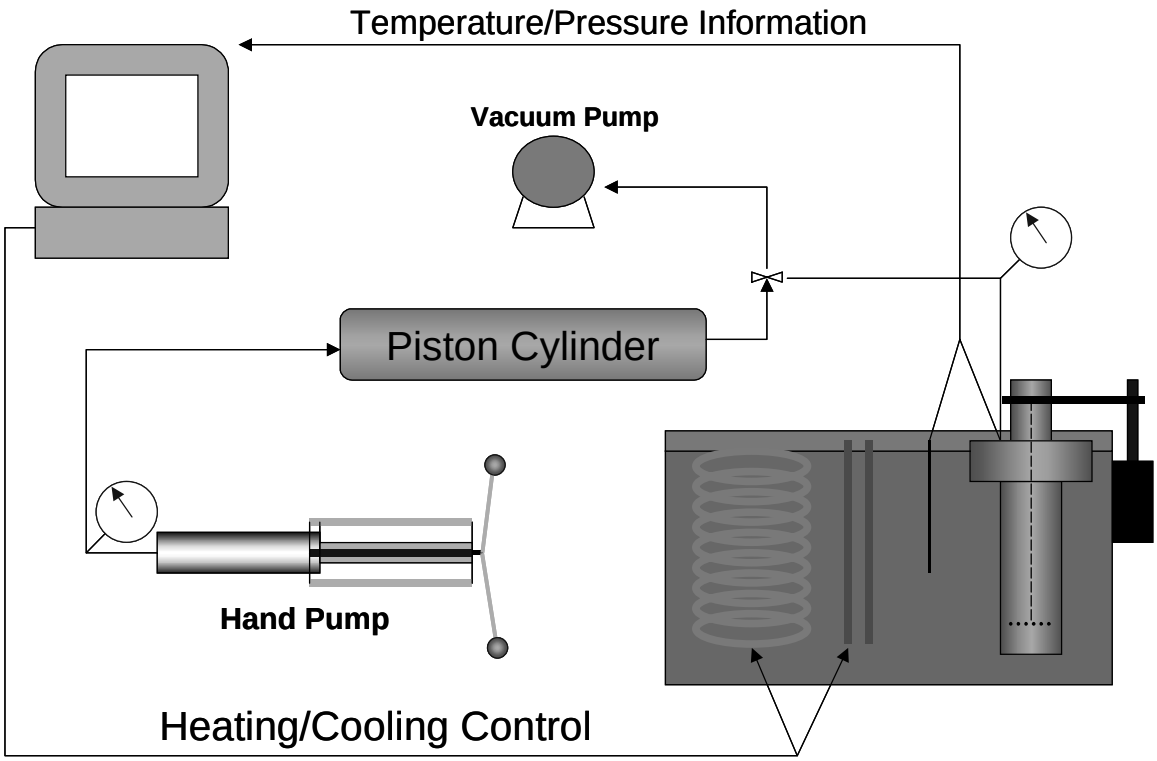

Figure 1 Experimental Apparatus

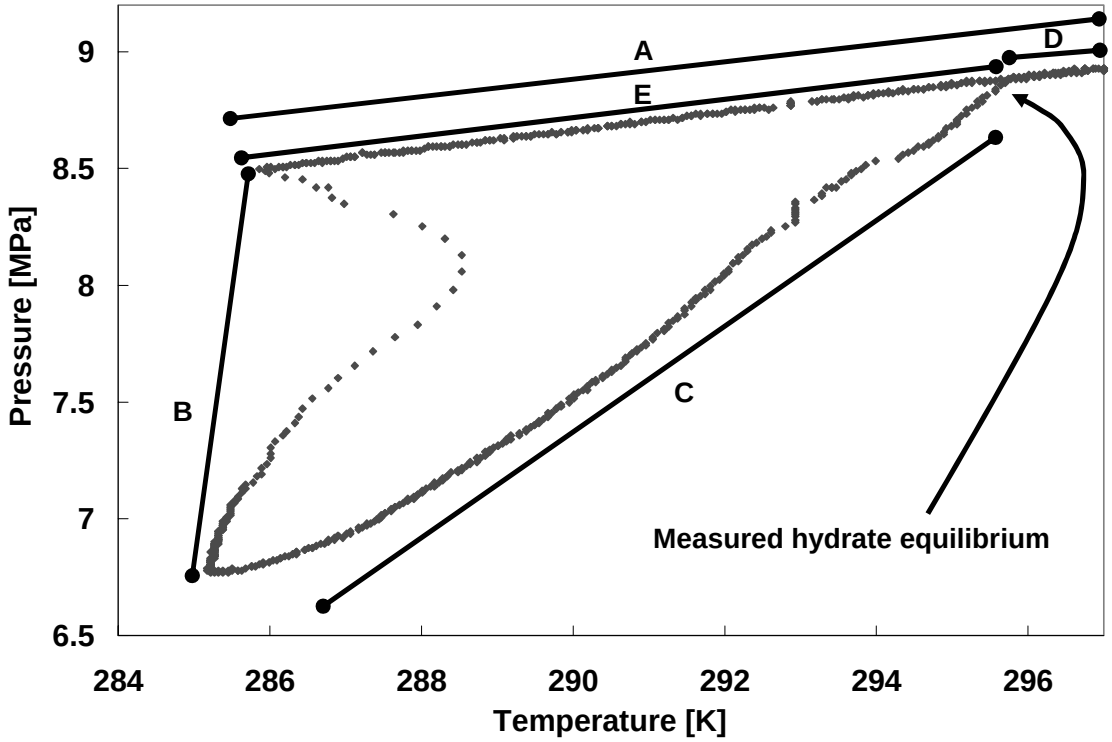

Figure 2 Pressure-Temperature Trace for Traditional Method

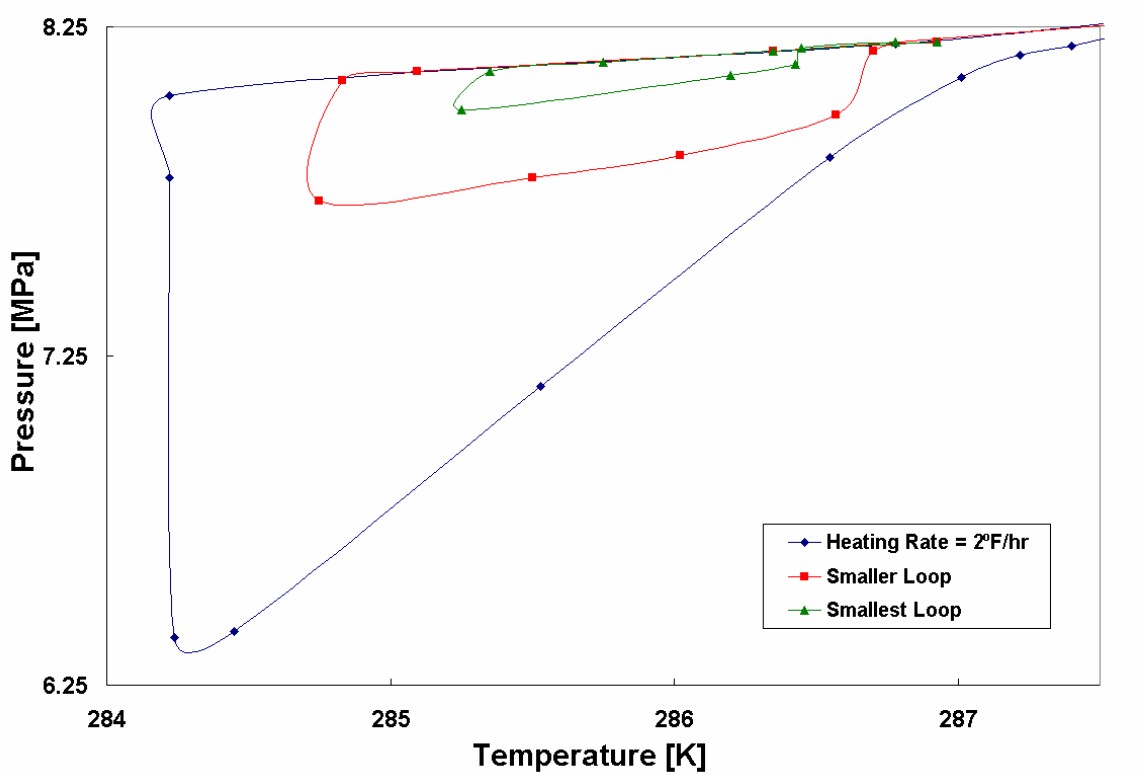

Figure 3 Smaller Pressure-Temperature Traces Using the New Experimental Method

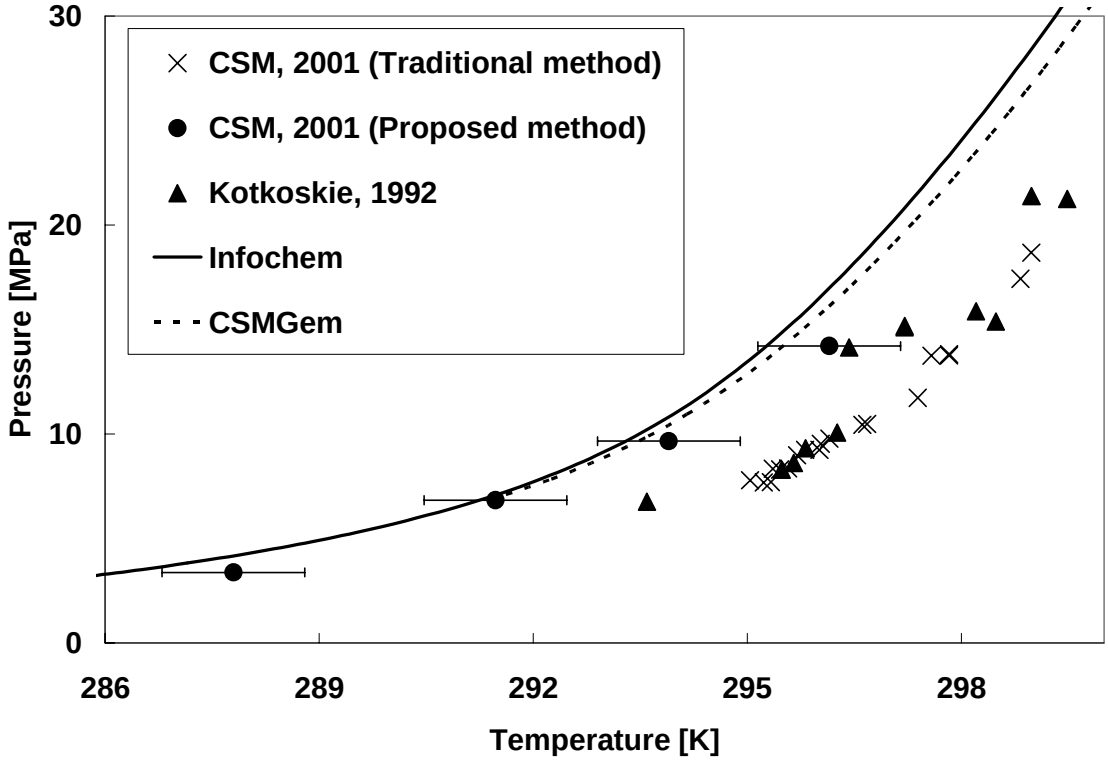

Figure 4 Green Canyon Gas Results

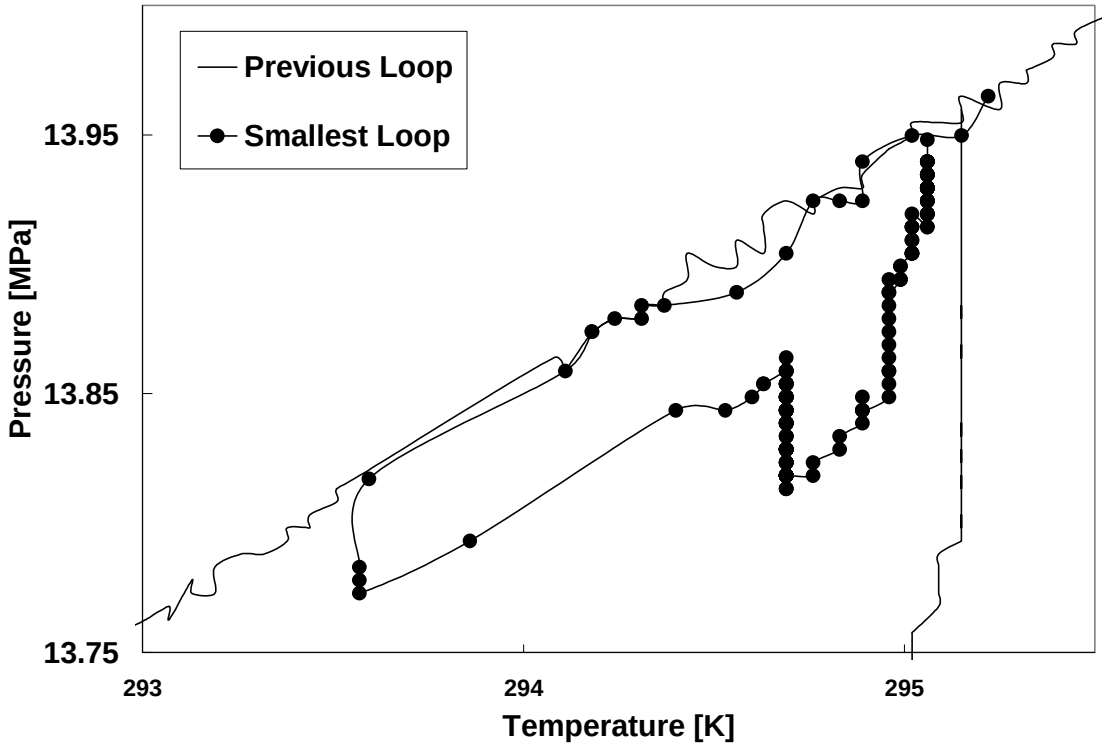

Figure 5 Pressure-temperature trace for the Green Canyon Gas

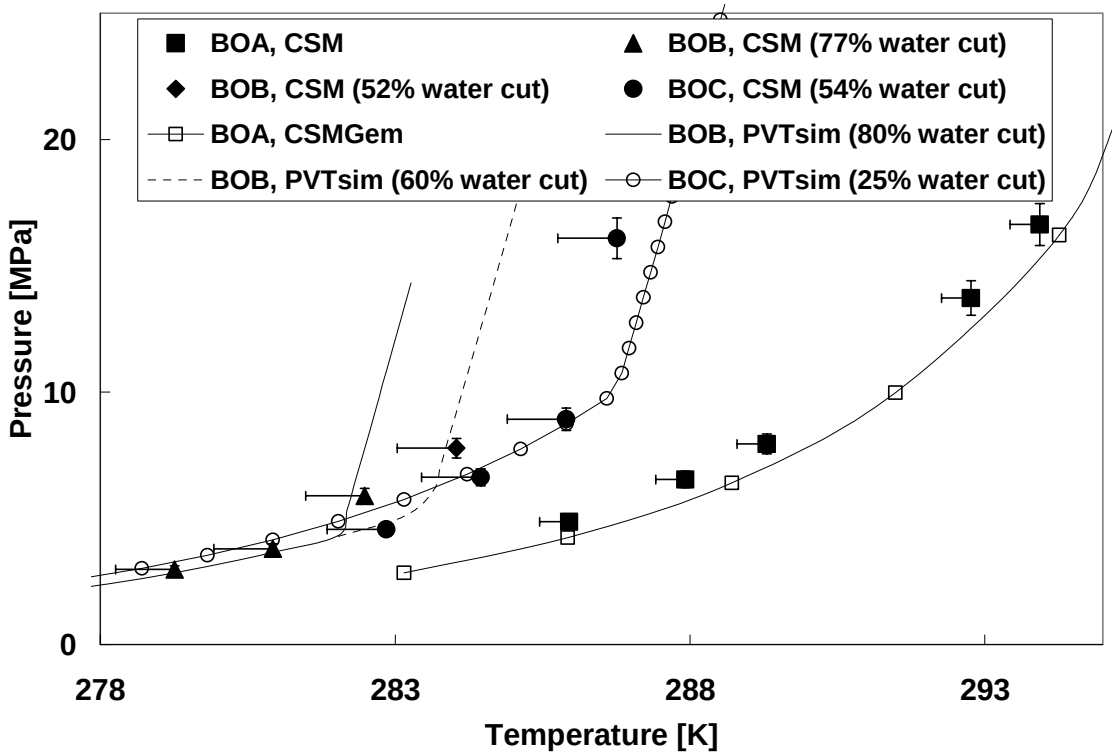

Figure 6 Black Oil Results

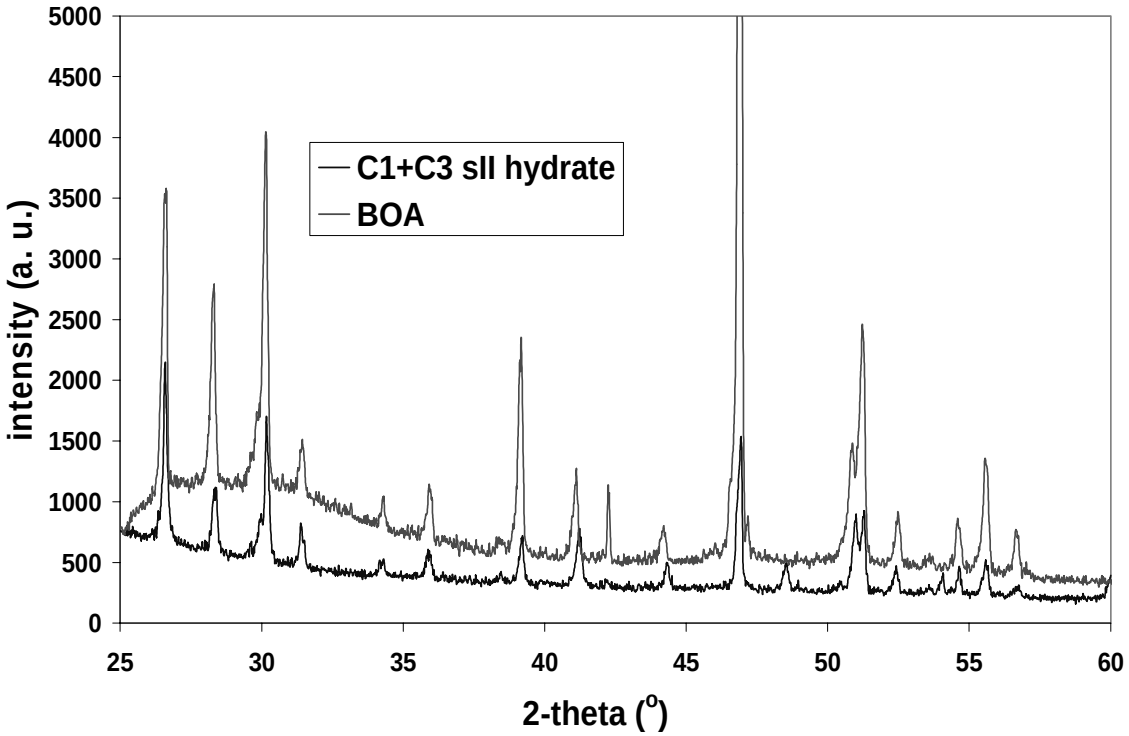

Figure 7 XRD Pattern for BOA Hydrate vs. C_1+C_3 sII Former

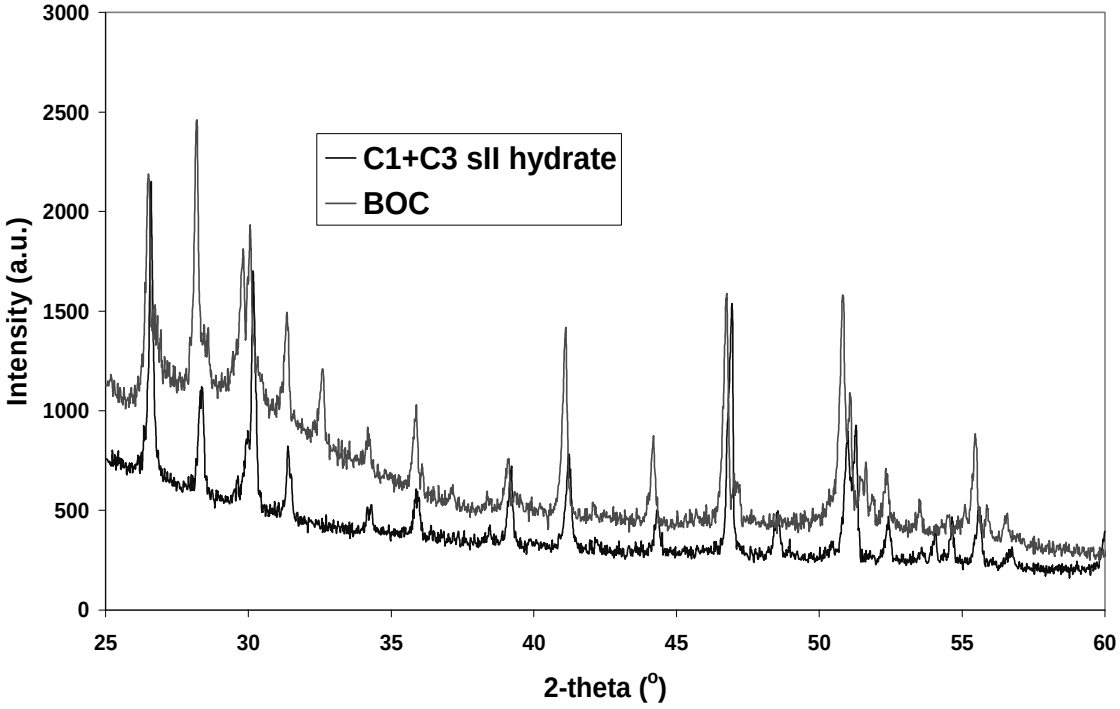

Figure 8 XRD Pattern for BOC Hydrate vs. C_1+C_3 sII Former

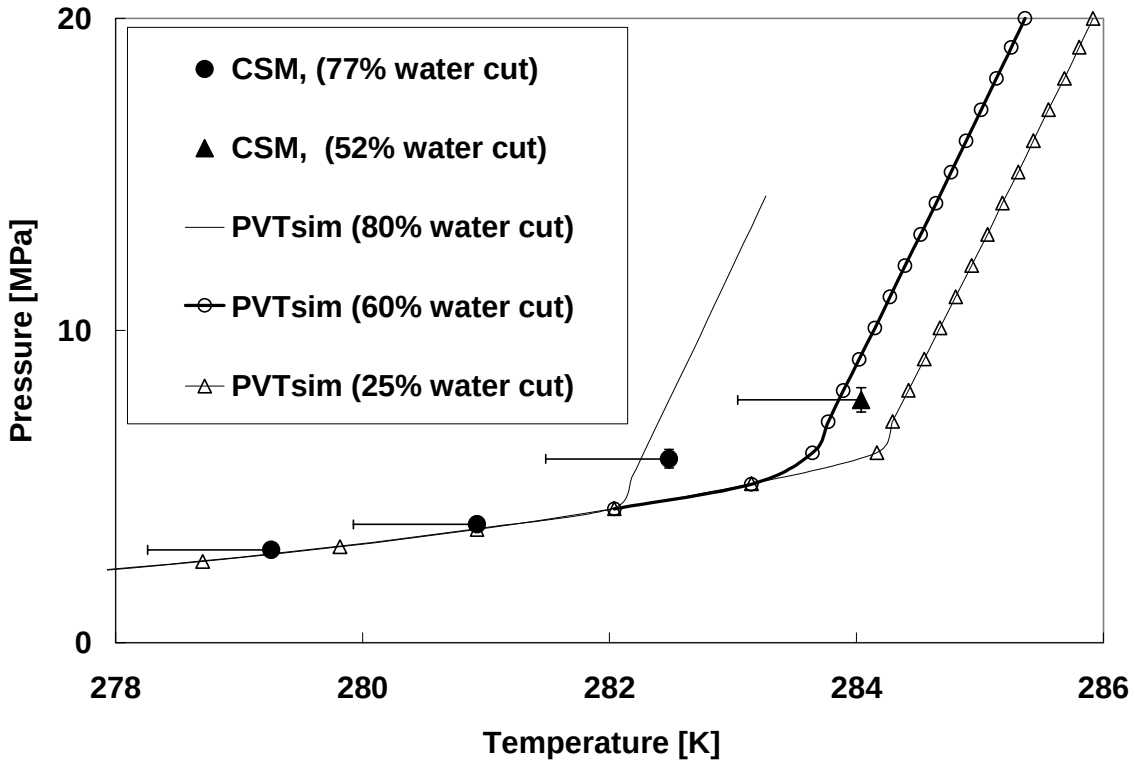

Figure 9 Black Oil B Results

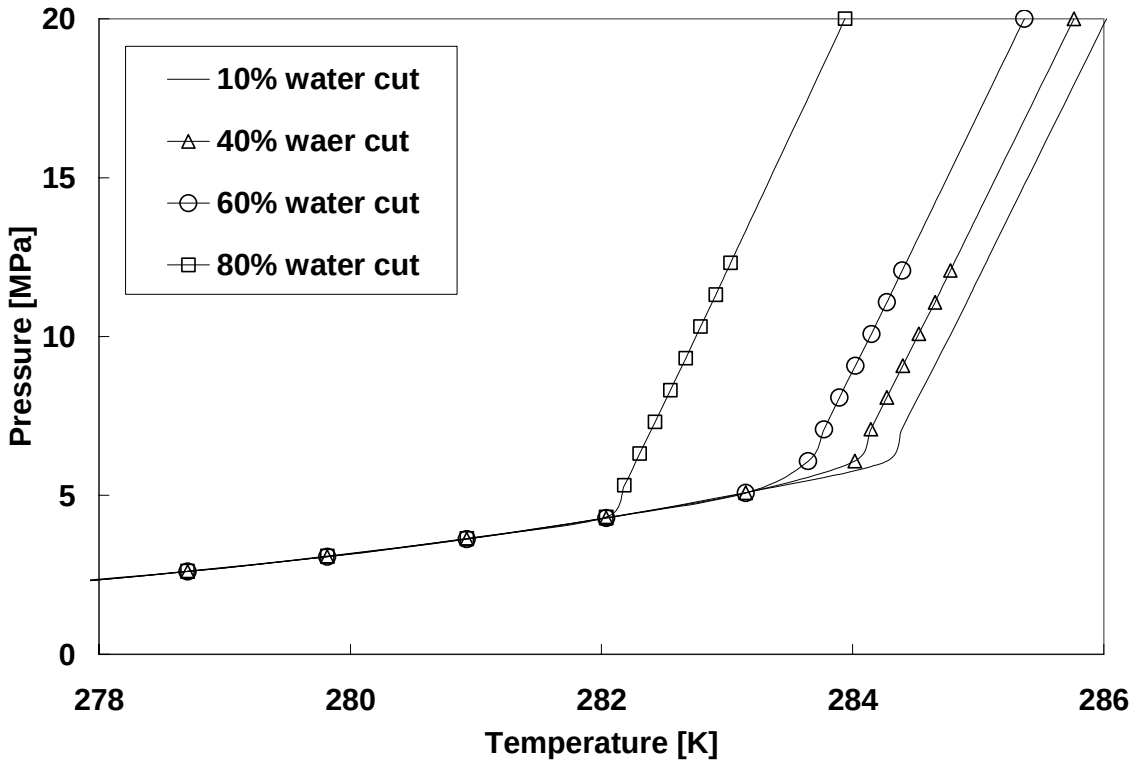

Figure 10 PVTsim Prediction of Black Oil Hydrate Equilibrium at Various Water Cuts